Journal of the Korean Vacuum Society
Vol. 5, No. 1, March 1996, pp. 25~32

An ERD-TOF System for the Depth Profiling of Light Elements

Y. S. Kim, H. J. Woo, J. K. Kim, D. K. Kim, H. W. Choi and W. Hong

Korea Institute of Geology, Mining and Materials
Gajung-Dong 30, Yusong-Ku, Taejon
(Received September 18, 1995)

경원소 적층 분석을 위한 탄성되튐-비행시간 측정시스템

김영석 · 우형주 · 김준곤 · 김덕경 · 최한우 · 홍 완

한국자원연구소, 방사화분석연구그룹
(1995년 9월 18일 접수)

Abstract – An ERD-TOF system is constructed for the nondestructive depth profiling of light elements in thin films in the range of several thousand angstroms. The particles, recoiled by 10 MeV ^{35}Cl projectiles, were detected by a Time-Of-Flight spectrometer composed of a MCP (Micro Channel Plate) and a SSB (Silicon Surface Barrier) detector. A two parameter data acquisition system composed of two PC's was constructed for registering simultaneous time and energy signals. A Si_3N_4/poly-Si/SiO_2/Si sample was analyzed and the result is compared with RBS. The detection limit, maximum probable depth and depth resolution for light elements in silicon are about 4×10^{14} atoms/cm^2, 5,000 Å and 100 Å, respectively.

요 약 – 탄성되튐-비행시간 측정법에 의하여 박막 중 수천 Å 내의 탄소, 질소, 산소 등 경원소의 깊이방향 농도를 비파괴 측정할 수 있는 씨스템을 제작하였다. 입사입자로는 10 MeV의 ^{35}Cl을 사용하였으며, 입사입자에 의하여 되튀는 시료내 입자의 비행시간 및 운동에너지는 MCP(Micro Channel Plate)와 SSB(Silicon Surface Barrier) 검출기로 구성된 비행시간 측정기에 의하여 측정하였다. 한 사건에 대한 두개의 동시정보를 기록하기 위하여 2대의 PC를 이용한 2변수 데이터 처리 시스템을 제작하였으며 2차원 display 프로그램을 제작하였다. Si_3N_4/poly-Si/SiO_2/Si 표준박막을 시험분석하였으며 결과를 RBS 분석결과와 비교하였다. 이 시스템에 의한 경원소의 검출한계는 실리콘매질에서 대략 4×10^{14} atom/cm^2, 검출가능깊이는 약 5,000 Å, 깊이분해능은 100 Å이다.

1. Introduction

The content of light elements such as carbon, nitrogen and oxygen plays an important role on the electrical, chemical and mechanical property of thin film materials like semiconductors, superconductors, magnetic and optical storage devices and surface hardened metals. The analysis of those elemental concentrations is, therefore, of crucial importance. SIMS, AES or ESCA can be used for the purpose, but they are all at best semi-quantitative tools. RBS is well known for its good quantitativeness, but is not applicable in a case where light elements in a heavy matrix should be analyzed-which is unfortunately the normal situation.

The ERD (Elastic Recoil Detection) method is a good complement to RBS which was tried firstly by Cohen [1] in 1972 and by L'Ecuyer [2] in 1976 for the detection of hydrogen and lithium. Since then, almost all laboratories in possession of small electrostatic accelerators have employed the method. The detection of such very light elements may be performed with very simple detection system like in the RBS just by adding absorber foils in front of a charged particle detector in order to

remove the heavier projectiles [3]. But this simple method cannot be used where somewhat heavier elements (B to F) should be analyzed, because those elements cannot be distinguished from the projectile or matrix elements in the energy spectrum by the use of absorber foils. Instead of absorber foil technique, many efforts have been put to detect and identify the recoiled particles [4]. Among them, TOF (Time-Of-Flight) spectrometer can be used where projectiles of energy 10~20 MeV are available. The spectrometer consists usually of a start and a stop detector. The start and stop detectors should have very good time response property: usually time resolution of less than 1 ns FWHM. In many cases the stop detector serves also as the energy detector which registers the kinetic energy of the projectile. The mass can, then, be calculated from the TOF and energy for every single event. The depth profiles of target elements are obtained from the mass-separated energy spectrum.

We have constructed an ERD-TOF spectrometer at the KIGAM 1.7 MV Tandem Accelerator Laboratory. The start detector consists of a thin carbon foil, accelerating electrodes and a MCP (Micro Channel Plate). A low ohmic SSB (Silicon Surface Barrier) detector was used both as the stop detector and the energy detector. The simultaneous time and energy signals from the detectors were then registered by the two parameter data acquisition system composed of a 8255A parallel interface chip and two PC's. A two dimensional display program was developed for the analysis of data. The performance of the system was tested by a standard sample.

2. Kinematics and Cross Sections

The collision of the incident particle of mass m and the target nucleus of mass M can be described fairly well by the coulomb interaction within the projectile kinetic energy range of several MeV to several tens MeV. The scattering (K) and recoil kinematic factor (Λ) in a geometry defined in Fig. 1 is given by

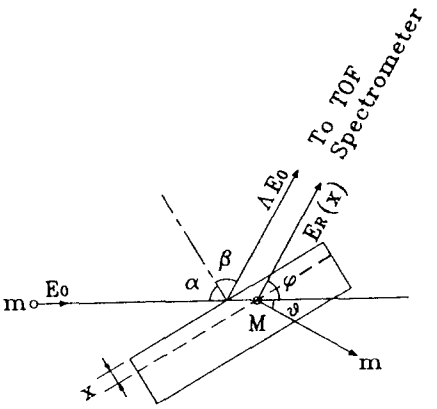

Fig. 1. Schematic diagram of the elastic recoil detection experiment.

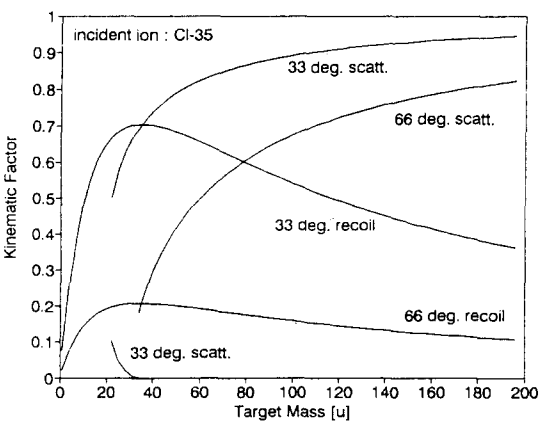

Fig. 2. Recoil and scattering kinematic factors for the recoil angles of 33° and 63° for incident ^{35}Cl beam.

$$K = \left(\frac{m\cos\theta \pm \sqrt{M^2 - m^2\sin^2\theta}}{M+m} \right)^2 \tag{1}$$

$$\Lambda = \frac{4mM}{(m+M)^2}\cos^2\phi, \tag{2}$$

where θ is the scattering angle and φ is the recoil angle in the laboratory frame. Fig. 2 shows the re-

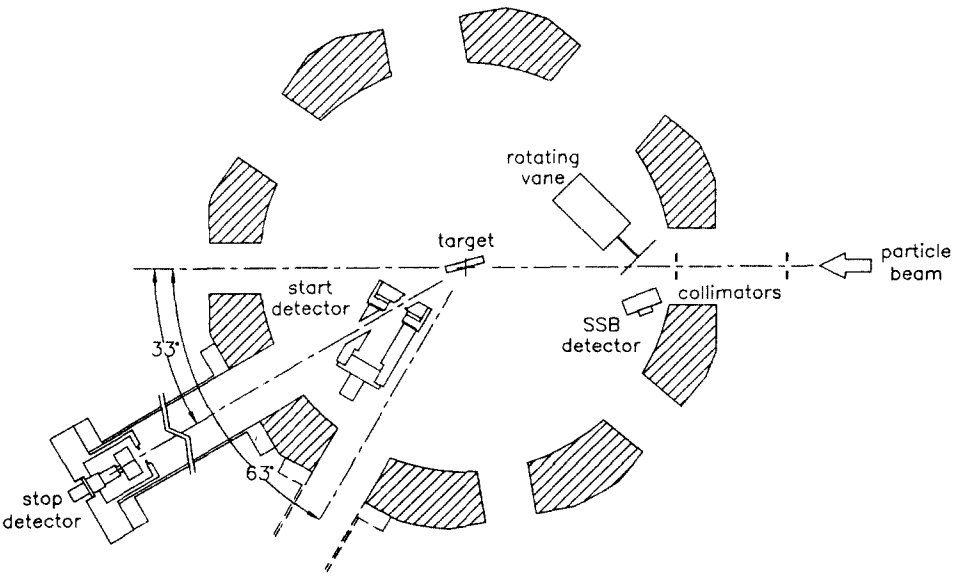

Fig. 3. Schematic diagram of the ERD-TOF spectrometer.

coil and scattering kinematic factors as a function of target mass for ^{35}Cl projectile. It can be seen that at $\phi = 33^\circ$ two scattering energies are possible when m>M. The recoil energy is, however, unique at given target mass. It is noteworthy from eq. (1) that a critical scattering angle exists when m>M:

$$\theta_{crit} = \sin^{-1}\left(\frac{M}{m}\right) \tag{3}$$

For example for ^{28}Si target the ^{35}Cl projectile cannot be scattered to $\theta > 53.1^\circ$. The existence of θ_{crit} is significant because it means if we place a detector at a recoil angle $\phi > \theta_{crit}$ we can avoid the projectiles falling into the detector.

Under the assumption that the projectile energy is large enough to avoid screening effect, the differential recoil cross section $\frac{ds}{d\Omega}$ is given by

$$\frac{ds}{d\Omega} = \left(\frac{z_1 z_2 e^2}{4E}\right)^2 \frac{4}{\cos^3\phi}\left(\frac{m+M}{M}\right)^2, \tag{4}$$

where z_1 and z_2 are the nuclear charges of projectile and target nucleus. As the incident energy E becomes smaller, the screening effect plays an important role and the cross section becomes accordingly smaller than is predicted by eq. (4). [5] Eqs. (2), (3) and (4) are important basic equations in the ERD-TOF experiment. The detector position should be decided by the compromise between the recoil energy ΔE and the cross section which are proportional to $\cos^2\phi$ and $\cos^3\phi$, respectively. Since the recoiled particles to be detected are heavy ions and have short ranges in detector materials, it is generally advantageous to have as large recoil energy as possible.

The analysis of ERD spectra is usually done by computer programs such as SENRAS [6].

3. The ERD-TOF Spectrometer

The ERD-TOF spectrometer is depicted in Fig. 3. The beam arrives at the target through the collimator unit. The beam size at the target can be adjusted to be 1~2 mm. For the purpose of current monitoring, a rotating vane was installed right after the collimator unit. The surface of the vane was coated with 200 Å Au. The backscatterd particles

were detected with a SSB detector. The target holder is made to be rotatable around its vertical axis. The start detector is located in the vicinity of the target and can be rotated around the target holder. The stop detector can be installed at the recoil angle $\phi = 33^\circ$ and 63°. The flight length can be adjusted to be 30, 60 and 100 cm. A low ohmic SSB detector (Ortec BF-18-100-60, USA, nominal resistivity : 500 Ωcm) was used as the stop detector and energy detector. The detailed description of the spectrometer can be found in ref. [4].

3.1. Start detector

The schematic diagram of the start detector is in Fig. 4. The recoiled particles pass through a 10 μg/cm^2 thick carbon foil. The electrons which are kicked out by the energetic heavy ions are accelerated by the accelerating electrode and fall into the two stage MCP (Hammamatsu F-4665-10, Japan, effective D=14.5 mm, G_{max}=5x10^7). The electrons are, then, multiplied and their signal is collected by the anode right behind the MCP. The extremely fast signal of the MCP ensures the intrinsic time resolution of the MCP to be less than 100 ps. The shape of the start detector is different from the conventional grid type [7] or coaxial type [8] start detectors. The grid type has the problem that the recoiled particles absorbed or scattered by the grid resulting in the distortion of the spectrum. The coaxial type has solved this problem but has a serious disadvantage that the produced electrons have different probabilities of reaching the MCP depending on the radial position of their production. Our MCP has overcome those two problems at the sacrifice of the small uncertainty of the start detector position (~1 mm). But the contribution of this uncertainty to the overall time resolution is negligible because the flight length is usually longer than 30 cm and the velocity of the recoiled particles are normally less than 1 cm/ns. In our type the most important factor in the design

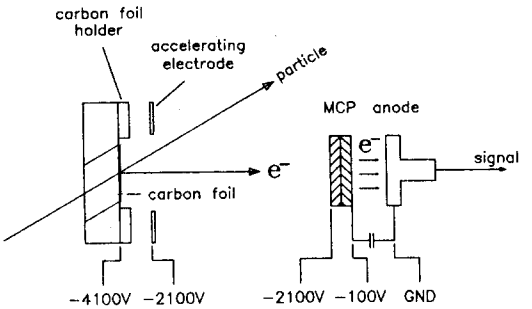

Fig. 4. Schematic diagram of the start detector.

is the shape of the accelerating electrode. Note that in Fig. 4 the carbon foil is surrounded by a certain thickness of foil holder. The shape of this holder, the accelerating electrode and the distance between them are the crucial design parameter of the start detector. Ideally, they should be constructed in the way that the ejected electrons make a parallel trajectory to the MCP. Simulation test shows the characteristics of the start detector as follows:

1) The electron flight time: 2.63±0.01 ns

2) The change in the flight time when the inner diameter of the carbon foil holder is in(de)creased by 1 mm: 100 ps

3) The change in the flight time when the inner diameter of the accelerating electrode is in(de) creased by 1 mm: 40 ps

4) The change in the flight time when the accelerating potential is in(de)creased by 10 V: 10 ps

5) The maximum change of the flight time when electron energy changes from 0 to 5 eV and the emission angle changes from 0° to 90°: 50 ps.

6) The change of the falling spot of a recoiled particle (6 MeV ^{12}C) due to the electrical field of the start detector when the flight length is 1 m : 1 mm

Above test ensures that the time resolution of the start detector is well below 300 ps which is the design criteria.

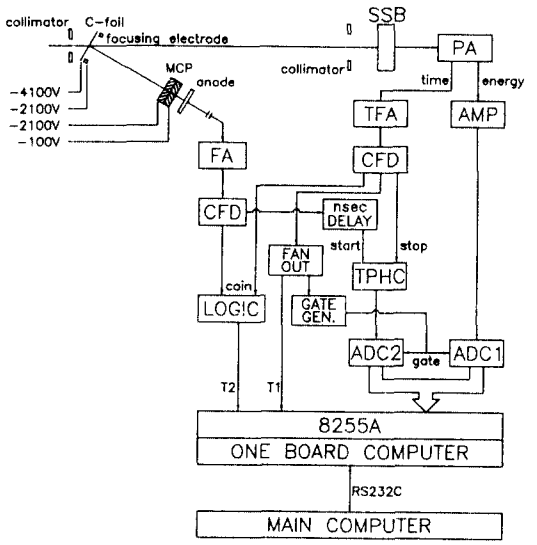

Fig. 5. Schematic diagram of the electronics and data acquisition system.

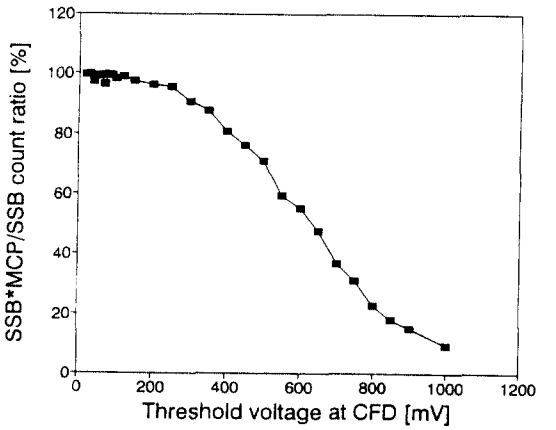

Fig. 6. The efficiency of the start detector as a function of the threshold voltage at the CFD for 0.2~2 MeV Si particles.

3.2. Electronics and two parameter data acquisition system

The electronic circuit and the data acquisition system is shown in Fig. 5. The MCP signals are amplified and discriminated by a CFD. A logic signal is then fed into the start input of the TPHC (Time to Pulse Height Converter) while another signal makes the coincidence with the SSB signal. The time output from the preamplifier of SSB is also amplified and discriminated by a CFD, then fed into the stop input of the TPHC. TPHC output is registered by ADC2. Meanwhile, the energy output is amplified and fed into ADC1.

The data acquisition system consists of 2 ADC's, an interface board with 8255A, the V40 one board computer and the main computer which is a normal PC as in Fig. 5. The ADC's are commercial CANBERRA 8075 and 8255A board is homemade. The V40 is a simple PC which controls the 8255A and sends the collected data to the main computer. The 8255A board communicates with V40 via ISA bus. The readout routine is written in Quick Basic. The readout routine can be triggered either by SSB signal or MCP*SSB signal from the logic unit depending on the usage. The readout routine firstly activates a clock (not shown in the figure). This is needed to register the system dead time. Then, the routine reads brutally the pulse height information in the ADC's. During the readout, the ADC's are blocked to accept no more signals. At the end of the readout, the ADC's are reset and the the clock is disabled. The accumulated time in the clock is then the system dead time. When the amount of collected data set reaches a preset value, the data bunch is sent to the main computer through RS 232C port using the X00 low level serial I/O communication driver.

4. Test Experiment

4.1. Efficiency of the ERD-TOF spectrometer

The detection efficiency of the spectrometer is very important and is mainly the efficiency of the start detector. The efficiency depends on the number of electrons ejected from the carbon foil which is a function of the projectile charge and energy [9]. Under the assumption that the efficiency of the SSB detector is 100%, the efficiency of the start detector is defined as

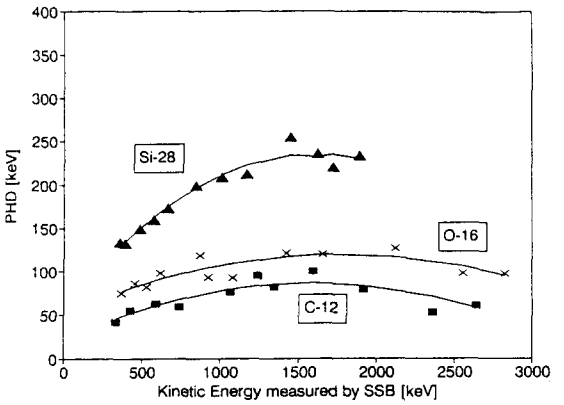

Fig. 7. PHD of the SSB detector used in the experiment for C, O and Si particles as functions of the kinetic energies. The lines are the result of the fitting by eq. (7).

$$\varepsilon = \frac{\text{count(MCP*SSB)}}{\text{count(SSB)}}, \quad (5)$$

where * means the coincidence. The detection efficiency was measured with recoiled Si particles by 10.2 MeV ^{35}Cl beam. The recoil energy of the Si particles were 0~2 MeV. Because of the cutoff of the SSB signals at the discriminator, the actual minimum energy of the Si particles was about 200 keV. Fig. 6 shows the efficiency as a function of the threshold voltage V_{th} at the CFD into which the MCP output signal is fed. The bias voltage at the MCP was 2000 V. It is seen that the efficiency is almost 100% at V_{th}<150 mV. In the real measurement, the V_{th} cannot be set too low because then the CFD can be triggered by noises which can result in the register of uncorrelated events (the events of which the start and stop signals are not correlated).

4.2. Pulse Height Defect of the SSB detector

It is well known that semiconductor detectors show pulse height defect (PHD) for heavy ions [10]. Therefore, in the most applications to heavy ions, the detectors are overbiased to reduce the effect with high electrical fields. Nevertheless, PHD becomes never zero and for any application PHD must be estimated precisely.

For the PHD measurement we used C, O ions scattered by Au and Si ions recoiled by Cl. Since the real energy of the ions can be precisely calculated from the TOF, the PHD can be easily measured by the following equation:

$$\text{PHD} = E_{TOF} - E_{SSB}, \quad (6)$$

where E_{TOF} is the energy measured by TOF and E_{SSB} is the energy registered by SSB detector. Fig. 7 is the PHD of the SSB detector for C, O and Si ions as functions of the kinetic energies. The lines are the fitting functions for the data points. The fitting function is selected empirically as

$$\text{PHD} = m^{2.3}\cdot(a + b\cdot E_{SSB} + c\cdot E_{SSB}^2) + d \text{ [keV]}. \quad (7)$$

The fitting parameters were found to be a = 0.0048, b = 0.00012, c = -4.43×10^{-8} and d = 50.

4.3. Test measurement

A test measurement was performed for a Si_3N_4/poly-Si/SiO_2/Si sample. 10.2 MeV ^{35}Cl beam was bombarded to the sample at an incident angle of 74°. The recoil angle was 33°. The trigger condition was the SSB signal alone. Fig. 8 shows the [E, T] and [E, m] spectra collected for 5 minutes at the flight length 60 cm. Since the recoil angle is less than the critical angle, Cl appears in the spectra. Note that N and O are well separated. The events scattered around the upper part is due to the random coincidence between start and stop signal. Those events can be avoided with a proper suppression circuit. The events at the upper most part are the events which lacks the MCP signal. Those events shows the efficiency of the MCP, and therefore, the on-line control of the efficiency is possible by checking the ratio between the number of MCP*SSB and SSB events at given measured energies. It was observed that the efficiency was better than 98% at the whole energy region.

The [E, m] spectrum was generated by the transformation of the [E, T] data by the kinetic en-

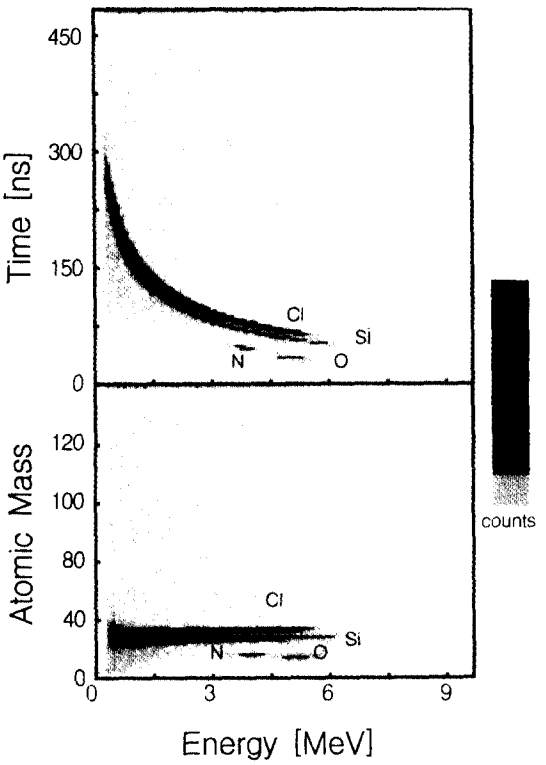

Fig. 8. The [E, T] (upper) and [E, m] (lower) spectra of the Si_3N_4/poly-Si/SiO_2/Si sample. See the text for the explanation.

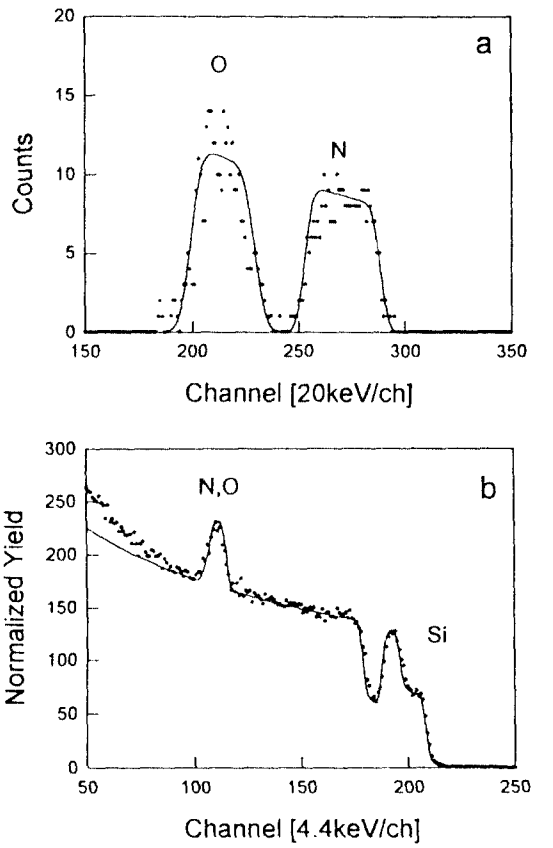

Fig. 9. (a) The ERD spectrum and (b) the RBS spectrum of the Si_3N_4/poly-Si/SiO_2/Si sample. The lines are the results of fittings by SENRAS and RUMP.

ergy equation and eq. (7). Since the PHD correction is not very precise, the transformation results in a slight error of the mass values. But it is not a problem in most cases because the species can be easily identified by the correlation. Once the masses are identified, the energy of every single data points are calculated again with TOF data because TOF data are preciser than SSB data.

The projection of the [E, m] spectrum on energy axis results in Fig. 9(a). The line is the result of the simulation by SENRAS program. It can be compared with the RBS spectrum for the same sample (Fig. 9(b)). When the contents of light elements are very large as in the case of this sample, RBS may be also used in the quantitative analysis as is clear in the figure. But normally for samples with light element content less than a few %, light elements are hardly recognized in RBS spectra. The line in the RBS spectrum is the result of the simulation by RUMP. The thicknesses for Si_3N_4/poly-Si/SiO_2 estimated by ERD-TOF and RBS are 350/240/300 and 400/220/300, respectively in the unit of 10^{15} atoms/cm^2. Since the RBS result is proven to be precise to about 5%, the ERD-TOF result indicates a small imperfectness in the measurement. One possible error can occur from the cross section formula we used because the screening effect may be somewhat large in the energy region we are working with, resulting in the smaller thickness than reality.

The time resolution of the spectrometer is about 400 ps at the moment. With about 50 keV energy

resolution for 1.68 MeV ^{14}N, the mass resolution is about 0.42 u FWHM. For ^{9}Be and ^{19}F the mass resolution is about 0.17 u and 0.7 u. The depth resolution for ^{16}O in Si recoiled by 10 MeV ^{35}Cl is about 50 Å at the target surface as is calculated from the energy resolution and geometrical broadening. It degrades to about 100 Å as the penetration depth increases due to the energy straggling and multiple scattering [11]. But in the reality, the resolution at the surface calculated from the leading edge of the spectrum in Fig. 9 is about 150 Å. This rather large discrepancy is due to the carbon contamination during the irradiation of the sample. The detection limit in the case of 1 hour measurement (total dose 1.2 μC) is about $4x10^{14}$ atoms/cm^2 for carbon, nitrogen and oxygen in silicon. This value can be compared with the detection limit of about 10^{17} atoms/cm^2 for normal RBS. The maximum probable thickness is roughly 5,000 Å depending on the sample tilting.

5. Conclusion

The ERD-TOF spectrometer was built for the depth profiling of light elements in thin films. The performance test shows its usefulness for the quantitative analysis with very good depth resolution. But the detection system together with its data acquisition system is somewhat too complicated for the routine analysis and should be improved. The carbon contamination was observed during the experiment and it should also be solved. The exact cross section data, which are currently very scarce, are required for the exact evaluation of the measurement. The mass and depth resolutions could be improved if the stop detector is replaced with another MCP. These improvements are in the progress.

Acknowledgement

This work was supported by the Korean Ministry of Science and Technology.

References

1. B. L. Cohen, C. L. Fink and J. H. Degnan, J. Appl. Phys. **43**, 19 (1972).
2. J. L'Ecuyer, C. Brassard, C. Cardinal, J. Chabbal, L. Deschenes, J. B. Labrie, B. Terreault, J. G. Mariel and R. St-Jacques, J. Appl. Phys. **47**, 881 (1976).
3. B. L. Doyle and P. S. Peercy, Appl. Phys. Lett. **34**, 811 (1979).
4. Y. S. Kim, N. B. Kim, H. J. Woo, J. K. Kim, D. K. Kim, H. W. Choi, W. Hong and S. Y. Choi, 'A Study on the Light Elements Analysis Technique Using Nuclear Reactions', MOST report KR-94(T)-14, (1994).
5. S. R. Lee and R. R. Hart, Nucl. Instr. and Meth. **B 79**, 463 (1993).
6. G. Vizkelethy, Nucl. Instr. and Meth. **B45**, 1 (1990).
7. S. Lunardi, M. Morando, C. Signorini, Fortuna, G. Prete, W. Starzecki and M. Stefenini, Nucl. Instr. and Meth. **196**, 223 (1982).
8. E. Weissenberger, W. Kast and F. Goennenwein, Nucl. Instr. and Meth. **163**, 359 (1979).
9. H. Rothard, K. Knoneberger, A, Clouvas, E. Veje, P. Lorenzen, N. Keller, J. Kemmler, W. Meckbach and K.-O. Groeneveld, Phys. Rev. **A41**, 2521 (1990).
10. H. W. Schmitt, W. E. Kiker and C. W. Williams, Phys. Rev. **137**, B837 (1965).
11. J. P. Stoquert, G. Guillaume, M. Hage-Ali, J. J. Grob, C. Ganter and P. Siffert, Nucl. Instr. and Meth. **B44**, 184 (1989).